

# Microwave Kinetic Inductance Detectors: The First Decade

Benjamin A. Mazin

*Department of Physics, University of California, Santa Barbara, CA 93106*

**Abstract.** Microwave Kinetic Inductance Detectors, or MKIDs, are non-equilibrium superconducting detectors made out of high quality factor superconducting microwave resonant circuits. Their primary advantage over other low temperature detector technologies is their built-in frequency domain multiplexing at GHz frequencies, allowing thousands of detectors to be read out through a single transmission line. MKIDs are now celebrating their tenth birthday, so this review aims to sum up what has been learned over the first decade and explore the diversity of current MKID projects.

**Keywords:** Microwave Kinetic Inductance Detectors

**PACS:** 85.25.Oj, 85.25.Pb

## INTRODUCTION

Microwave Kinetic Inductance Detectors (MKIDs) are a type of non-equilibrium superconducting photon detector [1, 2, 3]. The primary attraction of MKIDs is that, unlike many other low temperature detectors, they are easy to multiplex into large arrays [4, 5, 6].

MKIDs work on the principle that incident photons change the surface impedance of a superconductor through the kinetic inductance effect. The kinetic inductance effect occurs because energy can be stored in the supercurrent of a superconductor. Reversing the direction of the supercurrent requires extracting this stored energy, which yields an extra inductance. This change can be accurately measured using a thin film superconducting resonant circuit, resulting in a measurement of the energy and arrival time of the incident photon for the case of near-IR to X-ray photons, or the total photon flux for lower energy photons. The only real difference between arrays designed for different wavelengths is the method used to couple the photon energy into the MKID — the detectors themselves and the readout are nearly identical. The left side of Figure 1 gives an overview of this process. In Figure 1 panel (a), a photon with energy  $h\nu > 2\Delta$  ( $\Delta$  is the superconducting gap energy) is absorbed in a superconducting film cooled to  $T \ll T_c$ , breaking Cooper pairs and creating a number of quasiparticle excitations  $N_{qp} = \eta h\nu/\Delta$ . The efficiency of creating quasiparticles  $\eta$  will be less than one since some of the energy of the photon will end up as phonons. In this diagram, Cooper pairs (C) are shown at the Fermi level, and the density of states for quasiparticles,  $N_s(E)$ , is plotted as the shaded area as a function of quasiparticle energy  $E$ .

Panel (b) shows that the increase in quasiparticle density changes the surface impedance  $Z_s = R_s + i\omega L_s$  of the film (represented as the variable inductor), which is used as part of a microwave resonant circuit. The resonant circuit is depicted schematically here as a parallel  $LC$  circuit

which is capacitively coupled to a through line. The effect of the surface inductance  $L_s$  is to increase the total inductance  $L$ , while the effect of the surface resistance  $R_s$  is to make the inductor slightly lossy, adding a series resistance.

Panel (c) shows that on resonance, the  $LC$  circuit loads the through line, producing a dip in its transmission. The quasiparticles produced by the photon increase both  $L_s$  and  $R_s$ , which moves the resonance to lower frequency (due to  $L_s$ ) and makes the dip broader and shallower (due to  $R_s$ ). Both of these effects contribute to changing the amplitude (c) and phase (d) of a microwave probe signal transmitted past the circuit. The amplitude and phase curves shown in this illustration are actually the data measured for an aluminum test device at 120 mK (solid lines) and 260 mK (dotted lines), which is of a magnitude similar to what would be expected from a photon event. This choice of circuit design, which has high transmission away from resonance, is very well suited for frequency-domain multiplexing, since multiple resonators operating at slightly different frequencies can all be coupled to the same through line.

The primary advantage of MKIDs compared to other low temperature detectors such as superconducting tunnel junctions (STJs) [7, 8] or transition edge sensors (TESs) [9] is that by using resonant circuits with high quality factors, passive frequency domain multiplexing allows up to thousands of resonators to be read out through a single coaxial cable and a single low noise, high bandwidth cryogenic amplifier (Figure 1, right). Large arrays of MKIDs are significantly easier to fabricate and read out than any competing technology. They do not require any superconducting electronics, and their readouts can leverage the tremendous advances in room temperature microwave integrated circuits developed for the wireless communications industry[10].

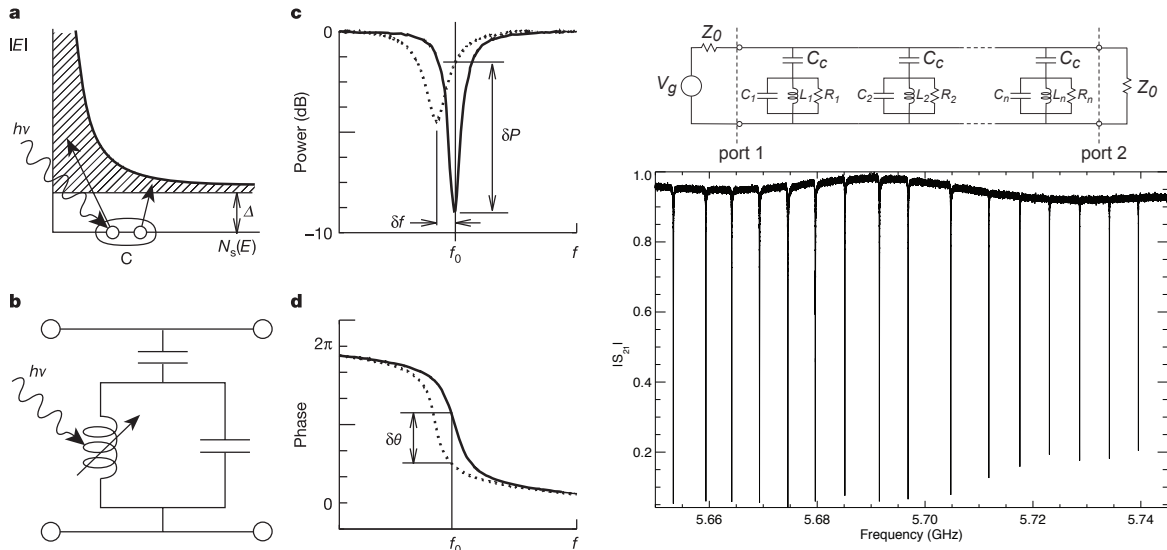


**FIGURE 1.** Left: An illustration of the operational principle behind a MKID. Right: An array of CPW MKIDs fabricated with a 40 nm aluminum film on sapphire show a mean frequency jitter of 0.8 MHz. This demonstrates that FDM multiplexing with a frequency spacing less than 2 MHz is feasible.

## IMPLEMENTATIONS

### Coplanar Waveguide and Microstrip Transmission Line Resonators

Coplanar waveguide (CPW) resonators were the first type of MKIDs to be studied in detail [1, 11] since they can be easily fabricated with a single metal layer on a crystalline dielectric. They consist of a CPW transmission line which is two slots cut into a metal ground plane to form a center strip, as shown in Figure 2. They are usually implemented as a quarter-wave transmission line resonator, capacitively coupled to a feedline on one end, and shorted on the other. Successful devices have also been made of half-wave resonators, with both ends open. CPW MKIDs are made mainly on high resistivity silicon or sapphire substrates. Successful CPW MKIDs have been made out of Nb, NbTiN, Ta, Re, Al, AlMn, Mo, PtSi, Ti, and Ir. Quality factors of up to several million are routinely observed in a subset of these materials. The primary drawback of CPW MKIDs, and transmission line resonators in general, is that the sensitivity to quasiparticles peaks in areas of high current. In the case of quarter wave resonators, this occurs near the shorted end of the resonator. The positional dependence means that a bare transmission line resonator is not a good detector — a separate structure, such as the antenna shown in Figure 11, is required to absorb the photons. The absorbed energy is then deposited into the sensitive end of the resonator. This sensitive end is often made of a lower gap material to increase sensitivity and act as a quasipar-

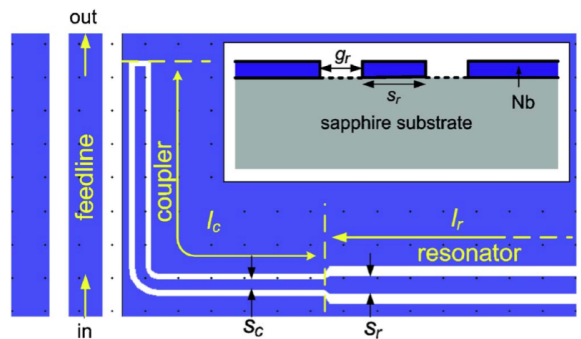


**FIGURE 2.** An illustration of the CPW coupler and resonator from Gao *et al.* [12]. The inset shows a cross-sectional view of the CPW. The contour of the metal surface and the contour of the exposed surface of the substrate are indicated by the solid line and the dashed line, respectively.

ticle trap to prevent diffusion of the quasiparticles away from the sensitive end of the resonator. This type of resonator, where a short length of the center strip near the short is a low gap superconductor, and the rest of the center strip and ground planes is a high gap superconductor, is referred to a hybrid resonator.

Due to noise and dielectric loss associated with amorphous thin film dielectrics (see below) less work has been done on microstrip transmission line resonators. In a microstrip, the transmission line is made of a stacked structure, with a dielectric separating two metal layers. Microstrip resonators are attractive in the near-IR through UV since they can be constructed on top of

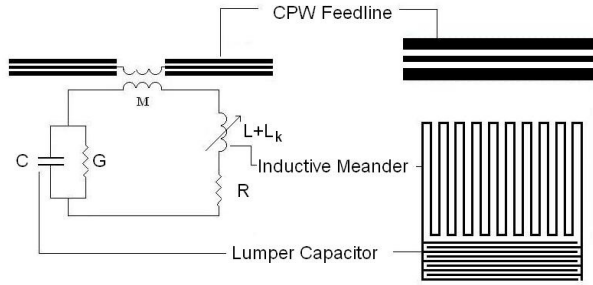


**FIGURE 3.** An example of a lumped element MKID from Doyle *et al.* [15].

other layers, allowing high fill factor 2-d arrays by hiding the resonators on top of the absorbers and illuminating through the substrate. Microstrip lines with thin dielectrics can also produce an extremely low phase velocity, allowing for very compact resonators. High quality dielectrics made of hydrogen rich amorphous silicon (aSi:H) have shown some promise, with internal quality factor  $Q_i > 2 \times 10^5$  at high readout powers, and NEPs around  $5 \times 10^{-17} \text{ W Hz}^{-1/2}$  [13].

Another possible approach aims to bypass the issues with deposited dielectrics by replacing the dielectric with vacuum. Work at Berkeley [14] has focused on constructing an air gap microstrip by pressing a patterned wafer onto another wafer with a solid ground plane. Figure 15 shows the relevant geometry.

### Lumped Element Resonators

A lumped element MKIDs (LEKID) [15] uses a separate inductor and capacitor to form a resonator. An interdigitated capacitor can be attached to an inductive meander to form a resonator, as shown in Figure 3. The inductive meander has a uniform sensitivity, and by adjusting the fill factor of the inductive meander, the normal state resistance of the metal in the meander, and adding a backshort it can be made to function as an efficient photon absorber. The frequency can be adjusted by changing the length of the inductive meander, and the coupling quality factor can be set by moving the device farther from the feedline. The advantage of lumped element MKIDs is that they are very simple to make since they do not require quasiparticle trapping. In the near IR through UV, this lack of quasiparticle trapping allows significantly higher theoretical (Fano) energy resolution for a given operating temperature.

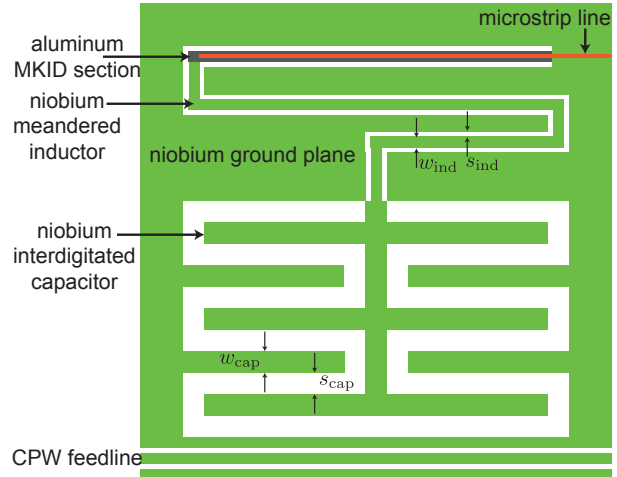


**FIGURE 4.** A mixed MKID with an interdigitated capacitor and CPW inductor from Noroozian *et al.* [16].

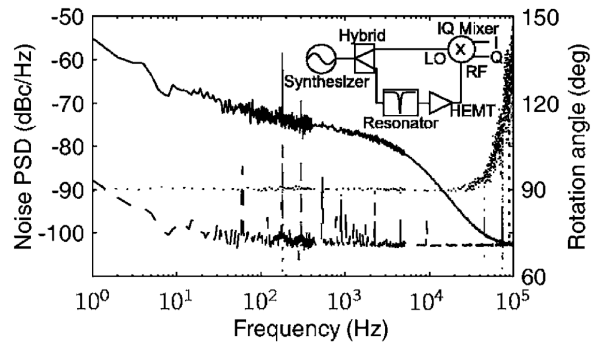


**FIGURE 5.** Noise spectra in the phase (solid line) and amplitude (dashed line) directions, from Gao *et al.* [17]. The noise data are from a Nb on Si resonator. The inset drawing shows the homodyne readout system used to obtain the data.

### Mixed Designs

There are other possible MKID designs using aspects of both lumped element and transmission line resonators. Recent work at Caltech [16], shown in Figure 4, has shown that a resonator with an interdigitated capacitor and a CPW inductor can drastically reduce the observed excess phase noise.

## LESSONS LEARNED

### Two Level System Noise

The primary source of the observed excess phase noise in MKIDs is caused by two level systems (TLSs) on the surfaces of the metals and dielectrics of the resonator [12,

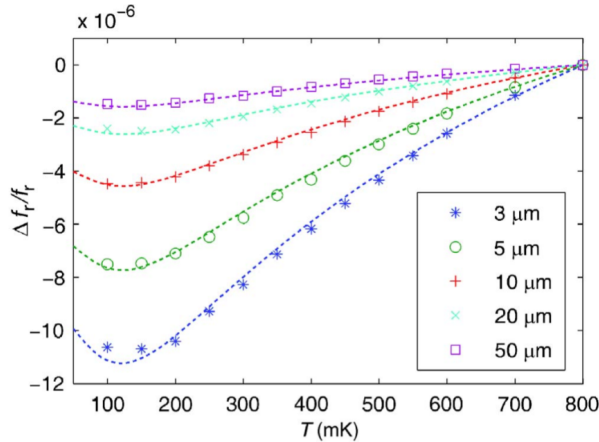


**FIGURE 6.** Fractional frequency shift as a function of temperatures from Gao *et al.* [12]. The different symbols show the fractional frequency shift of CPW resonators with different width center strips. The dashed lines indicate fits to TLS theory.

17, 18]. This noise is purely in the phase direction, as shown in Figure 5. This excess phase noise has a  $f_v = \nu^{-0.5}$  spectrum, and goes down as the microwave readout power is increased by  $f_v(P) = f_v P^{-0.5}$ . In Nb resonators, the excess noise has been observed to fall by a factor of 10 as the temperature is increased from 100 mK and 1 K [19]. Excellent agreement has been seen between the observed change in the resonant frequency at  $T < T_c/8$ , where no change is expected from BCS theory, and TLS theory, as shown in Figure 6.

Since the spectrum of the noise rises towards low frequencies, it is most dominant in observations that have a slow modulation frequency, such as submillimeter detectors. The excess phase noise comes from the capacitor, since it is the region with the highest electric field, while the kinetic inductance signal comes from the inductor. A clear trend has been seen where larger geometries result in lower excess phase noise, as shown in Figure 7. This can be understood in a simple way — since the TLSs are distributed on the surfaces, increasing the characteristic size  $l$  of the capacitor increases the volume the electric field samples by  $l^3$ , while the number of TLSs sampled only rises as  $l^2$ . By making the geometry of the capacitive section larger, TLS noise can be reduced significantly at the cost of a physically larger resonator.

MKIDs can be read out by measuring the phase change caused by the kinetic inductance effect, or by measuring the increased dissipation due to broken Cooper pairs. The phase response is usually  $\sim 4$  times greater than the dissipation response, but the excess phase noise can be large enough in some applications that a dissipation readout can provide better noise equivalent power (NEP). In many cases the optimum readout method will be a function of signal frequency, so most

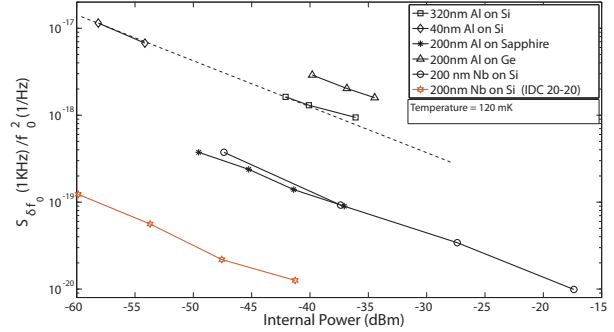


**FIGURE 7.** A plot of the excess fractional frequency noise for a variety of superconductors and substrates from Noroozian *et al.* [16]. All the data except the red points are from CPW resonators with a 3  $\mu\text{m}$  center strip and 2  $\mu\text{m}$  gaps. The red points are a mixed resonator with an interdigitated capacitor and CPW inductor, shown in Figure 4.

readouts are designed to record both the phase and dissipation response.

## Materials

For reasons that are not well understood, not all superconductors function well as MKIDs. Specifically, Mo and Ti films are very difficult to make into high quality factor resonators, and Ta films tend to not perform quite as well as Al and Nb.

Different substrates can dramatically affect the observed excess noise. We have seen sapphire wafers from different vendors give excess noises different by a factor of nearly 10. High resistivity silicon can perform nearly as well as sapphire if the native oxide is stripped off in a bath of hydrofluoric acid. Figure 7 shows a sampling of the measured noise for various metals and substrates [16].

## Lifetimes

The quasiparticle lifetime in superconducting films at temperatures well below  $T_c$  does not conform well to theoretical predictions [20]. Experiments at SRON have shown that reducing the flux of stray blackbody radiation absorbed in the resonator both directly and through the coaxial cables increases the observed lifetimes [21]. Experiments at Delft [22] have shown that the quasiparticle lifetime is related to disorder of the film. This was done by implanting Mn and Al ions into Al resonators. While increasing Mn concentration lowered  $T_c$  and increasing aluminum concentration did not, changes in the lifetime of similar magnitude were observed from implantation of either ion.

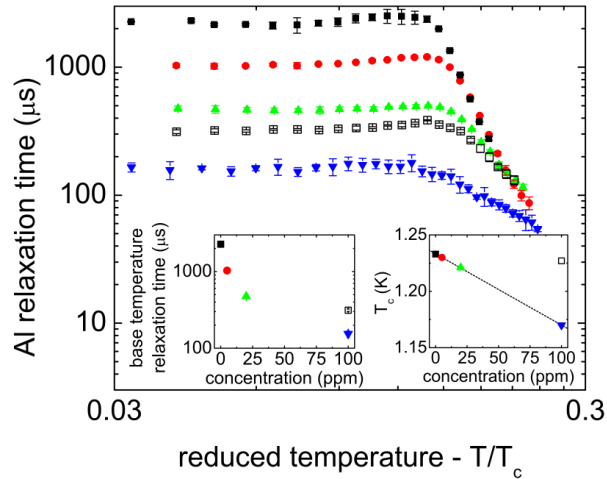


**FIGURE 8.** The quasiparticle lifetime as a function of the reduced bath temperature in Al with various ion-implanted concentrations, from Barends *et al.* [22].

## Readouts

In order to read out an MKID array, one must generate a comb of frequencies with a sine wave at the resonant frequency of each individual resonator. This comb is then sent through the device, where each detector imprints a record of its illumination on its corresponding sine wave. The comb is then amplified with a cryogenic amplifier and brought outside the cryostat. The comb is then digitized, and the phase and amplitude modulation of each individual sine wave is recovered in room temperature electronics. Aside from a simple cryogenic amplifier, there are no cryoelectronics. Compared to existing low frequency TES SQUID multiplexers, much of the complexity is moved from the base temperature to room temperature, where the full power of modern microwave electronics is available.

The technique described above, where a comb of frequencies is created, modified, then digitized and analyzed, is very common in modern wireless communications, where it is usually referred to as software-defined radio (SDR) [10]. A collaboration of nine universities and industrial partners has been formed to build an open source resonator readout around the Berkeley CASPER group's hardware. The chosen implementation is shown in Figure 9. In this implementation, dual 550 MHz, 16-bit digital to analog converters play back a pre-computed sine waves to generate the comb. Since two D/As are used, an IQ modulator allows the production of signals within a 550 MHz wide band centered on the LO frequency (usually 2–12 GHz). After the comb passes through the detector, it is mixed back down to baseband with another IQ modulator, low pass filtered, then digi-

tized with dual 550 MHz, 12-bit analog to digital converters. After digitization, the signals are passed to a fast field programmable gate array (FPGA). There are many algorithms that can be run in the FPGA to demodulate, or channelize, the signals. The simplest is a direct digital downconverter (DDC) that simply digitally multiplies the complex input signal by a sine wave at the desired frequency. This shifts the frequency of interest to 0 Hz. A digital filter followed by decimation gives the desired output data stream. The collaboration will likely use a more complex two stage channelization core that uses a polyphase filter bank (PFB) followed by a time-multiplexed direct digital downconverter to allow the readout of 128–256 resonators in 550 MHz of bandwidth. An alternative channelizer scheme involving a fast FFT spectrometer has been developed by SRON [23].

## CURRENT WORK

### Millimeter and Submillimeter Arrays

Detectors and instruments for millimeter and submillimeter astronomy is the most active current area of MKID research, with several groups in both the US and Europe actively developing detectors and instruments.

The first MKID instrument to be put on the sky, named DemoCam, was brought to the 10-m Caltech Submillimeter Observatory (CSO) in April, 2007 [24]. It consisted of a 16-pixel, 2 color/pixel array with a small SDR readout. Primarily a demonstration of the technology, DemoCam detected Jupiter within the first hours of being put on the telescope, and by the end of the run had detected the galactic ultracompact HII region G34.4 in both of its bands, as shown in Figure 10.

The MKID Camera project [25] is a collaborative effort of Caltech, JPL, the University of Colorado, and University of California Santa Barbara (UCSB) to develop a large-format, multi-color millimeter-wavelength camera for astronomy using MKIDs for the CSO. The camera will have 576 spatial pixels that image simultaneously in four bands at 750, 850, 1100, and 1300  $\mu\text{m}$ . It is scheduled for deployment at the CSO in the summer of 2010. Figure 11 shows the pixel design being pursued, which is a mixed resonator (an interdigitated capacitor and a CPW inductor) attached to a planar antenna array that forms a narrow beam without the use of optics.

SRON is developing a  $\sim 100$  pixel MKID demonstration array based upon single pixels consisting of an integrated MKID-antenna detector, with the antenna placed in the second focus of an elliptical Si lens. The design can be scaled to any frequency between 80 GHz and  $>5$  THz because there is no need for superconducting structures that become lossy at frequencies above the

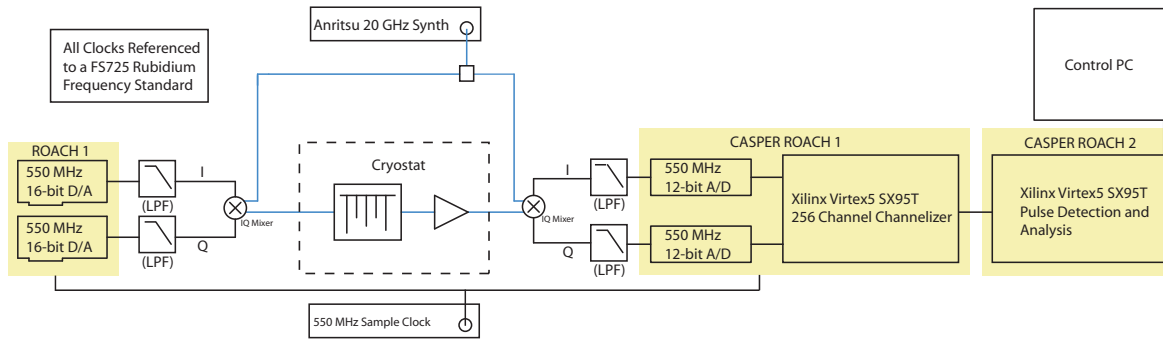


**FIGURE 9.** A block diagram of the Open Source Resonator Readout currently under construction. This readout will have final cost of about  $\sim \$35$  per resonator.

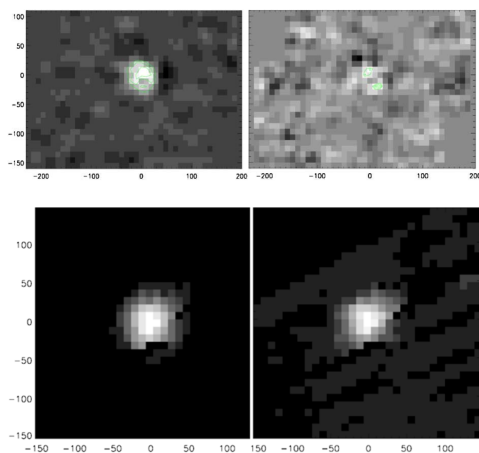


**FIGURE 10.** Image of G34.3 from two pixels in two colors during the same observation with DemoCam, from Schlaerth *et al.* [24]. This observation involved drift scanning over the source for roughly 20 minutes, leading to a detection at  $25\sigma$  at 240 GHz (left) and  $4.9\sigma$  at 350 GHz (right). Contours are at 10, 15,  $20\sigma$  and 3.5, 4,  $4.5\sigma$ , respectively. Below: an approximately 15 minute raster scan image of Jupiter at 240 GHz and 350 GHz, each detected at  $>1000\sigma$ . Map units are in arcseconds.

gap frequency of the materials used. Dark sensitivity of  $7 \times 10^{-19} \text{ W/Hz}^{1/2}$  using 100 nm thick Al devices and an optical coupling efficiency of 35% referring to the power of a single polarization optical signal in front of the Si lens of the detector have been demonstrated [27].

The University of Grenoble, SRON, Cardiff, Max-Planck Institute Bonn, and La Sapienza Roma are working on the Neel IRAM KIDs Array, or NIKA. The goal is to build a 50–200 pixels demonstration camera for October 2009 at the Pico Veleta 30-m dish. The collaboration is also working to develop large arrays of Lumped Element KIDs for millimeter wave detection, and are also using NbN and Nb high-Q resonators for fundamental studies on liquid helium hydrodynamics [28].

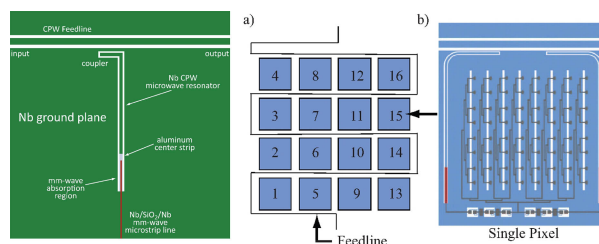


**FIGURE 11.** A schematic of the detector design for MKID-Cam, a 600 pixel, 4 color per pixel camera for the CSO from Maloney *et al.* [25]. A CPW MKID couples to a planar antenna array through a microstrip coupler. A superconducting filter bank takes the broadband signal from the antenna and breaks it into four separate bands, allowing one antenna to simultaneously feed four different colors to the appropriate MKIDs.

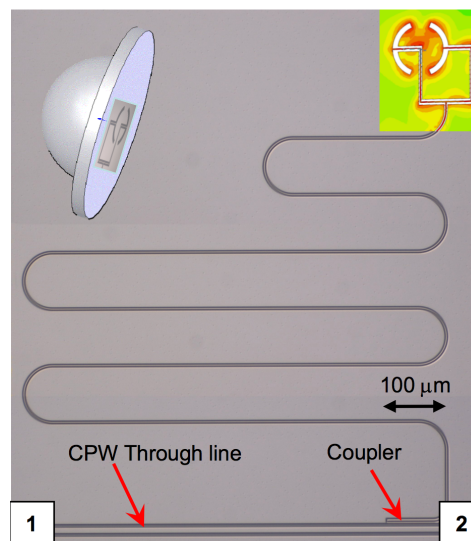


**FIGURE 12.** A single layer MKID submillimeter detector being developed by SRON from Yates *et al.* [27]. The device uses an elliptical silicon lens to focus light on the antenna, shown in color at the top right of the image.

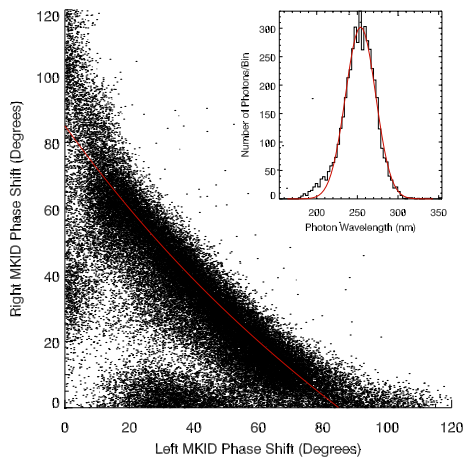


**FIGURE 13.** The response of a tantalum/aluminum optical strip detector to 254 nm UV light. Individual photons are plotted as points, where the x-axis shows the phase response of the left MKID, and the y-axis shows the phase response of the right MKID.

### Near Infrared to Ultraviolet Arrays

Strip detector arrays based on MKIDs are currently being developed by UCSB, Caltech, and JPL for near infrared to ultraviolet astronomy [3, 29]. Results from a functioning device are shown in Figure 13. These detectors will be used in the Array Camera for High-resolution Optical to Near-IR Spectrophotometry (ARCHONS) for the Palomar and Keck telescopes. ARCHONS will have over 1000 pixels, making it the largest optical/UV LTD camera by a factor of 10. It is expected to have a bandwidth of 350–750 nm, limited by the rising sky count rate towards the near infrared, and a field of view of approximately  $7 \times 21$  arcseconds. It is expected to achieve an energy resolution  $R = E/\delta E > 20$ .

### Dark Matter Detectors

The Caltech and Berkeley dark matter groups are pursuing two different approaches to using MKIDs for future cryogenic dark matter detectors. MKIDs are an exciting option for future cryogenic dark matter searches since the searches will require a very large numbers of high mass detectors. Caltech is pursuing a conventional CPW design using large aluminum fins as quasiparticle collectors [30], as shown in Figure 14. Berkeley is working on a vacuum dielectric microstrip design, shown in Figure 15.

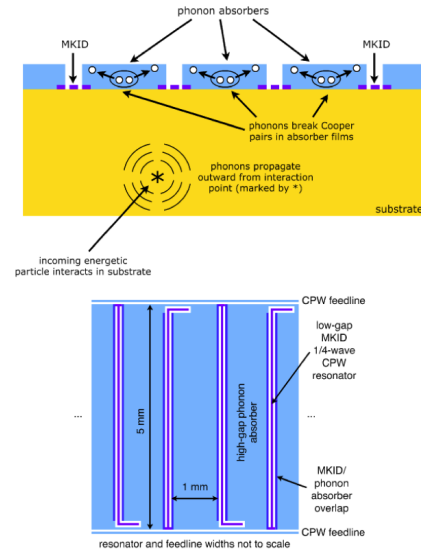


**FIGURE 14.** A cryogenic dark matter detector proposed by the Caltech group [30]. A dark matter particle interacting with a nucleon deposits energy in a crystal as phonons and ionization. The phonons are collected in thick aluminum film, then trapped in a lower gap (titanium) film that forms the ground planes of a CPW resonator. Ionization is detected by drifting the charge with an electric field.

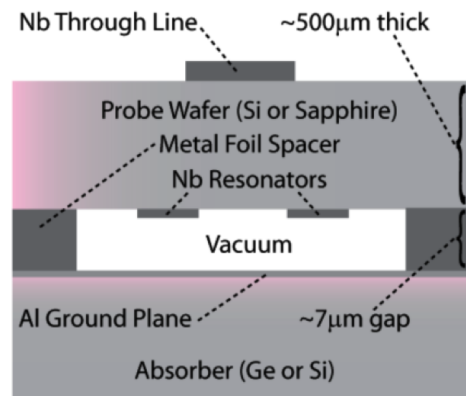


**FIGURE 15.** A cryogenic dark matter detector proposed by the Berkeley group [14]. A vacuum dielectric microstrip is formed by bonding a readout wafer onto detector wafer containing a superconducting aluminum ground plane.

### OUTSTANDING ISSUES

One of the main outstanding issues with MKIDs relates to their performance under optical loading, although significant progress has been made [31]. In millimeter and submillimeter applications the measured dark NEPs often quoted will invariably degrade under optical loading, and the interaction of the readout photons with quasiparticles in the resonator can lead to complex effects. Un-

derstanding the performance of the devices under load gives a much more realistic picture of the ultimate performance.

For photon counting MKIDs, the main issues appear to be quasiparticle trapping in thin films [29]. Geometries which are very reliable when used in thick film X-ray detectors fail frequently when made into thin optical/UV detectors. New materials and fabrication techniques will likely overcome these issues.

Another issue that is poorly understood is the interaction of MKIDs with magnetic fields. MKIDs show significant frequency response to changes in the magnetic field normal to the metal surface. This can be a significant problem in applications that move a dewar in Earth's field. Understanding and minimizing the magnetic field response through design changes and magnetic shielding is an important part of achieving the predicted sensitivities.

## CONCLUSIONS

MKIDs have been on a growth trajectory for the last decade, and as the complexity and number of pixels in millimeter and submillimeter instrumentation continues to grow they only become a more attractive option. Figure 16 shows a plot of submillimeter instrumentation and the time it was deployed. MKIDs are currently capable of powering state-of-the-art instruments, both in number of pixels and in sensitivity, at a lower price and with significantly less focal plane and readout complexity than comparable TES-based instruments. As an example, MKIDCam is expected to have a mapping speed of  $\sim 0.5 \text{ deg}^2/\text{mJy}^2/\text{hr}$  [31], a significant fraction of the mapping speed of SCUBA-II, with twice the colors, and cost less than 10% as much. This cost and complexity advantage will likely continue to drive the growth of the field.

## ACKNOWLEDGMENTS

The author would like to thank his many colleagues for sending the information used to write this review. This material is partially based upon work supported by the National Aeronautics and Space Administration under Grant NNN06ZDA001N-APRA2 issued through the Science Mission Directorate.

## REFERENCES

1. P. Day, H. Leduc, B. Mazin, A. Vayonakis, and J. Zmuidzinas, *Nature* **425**, 817–821 (2003).

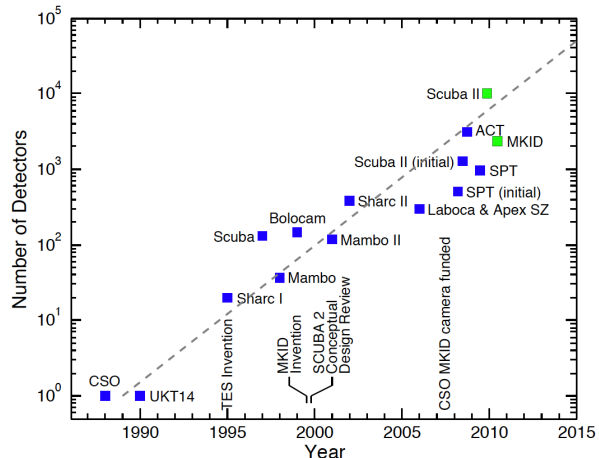


**FIGURE 16.** A plot from J. Zmuidzinas showing the number of detectors in millimeter and submillimeter astronomical instrumentation. Despite the youth of MKIDs, they are capable of producing instruments with state-of-the-art number of pixels at a significantly lower price than TES-based instrumentation like SCUBA-II.

2. B. A. Mazin, B. Bumble, P. K. Day, M. E. Eckart, S. Golwala, J. Zmuidzinas, and F. A. Harrison, *Appl. Phys. Lett.* **89**, 222507 (2006).
3. B. A. Mazin, M. E. Eckart, B. Bumble, S. Golwala, P. K. Day, J. Gao, and J. Zmuidzinas, *J Low Temp Phys* **151**, 537–543 (2008).
4. J. Chervenak, K. Irwin, E. Grossman, J. Martinis, C. Reintsema, and M. Huber, *Appl. Phys. Lett.* **74**, 4043–4045 (1999).
5. J. Zmuidzinas, and P. Richards, *Proc. IEEE* **92**, 1597–1616 (2004).
6. B. Mazin, P. Day, K. Irwin, C. Reintsema, and J. Zmuidzinas, “Digital readouts for large microwave low-temperature detector arrays,” in *Proceeding of LTD-11*, 2006, vol. 559 of *AIP Conference Proceedings*, pp. 799–801.
7. D. Twerenbold, *Europhys. Lett.* **1**, 209–214 (1986).
8. H. Kraus, F. Vonfeilitzsch, J. Jochum, R. Mossbauer, T. Peterreins, and F. Robst, *Physics Letters B* **231**, 195–202 (1989).
9. K. Irwin, G. Hilton, D. Wollman, and J. Martinis, *Appl. Phys. Lett.* **69**, 1945–1947 (1996).
10. B. Mazin, P. Day, K. Irwin, C. Reintsema, and J. Zmuidzinas, *Nucl Instrum Meth A* **559**, 799–801 (2006).
11. B. Mazin, *Microwave Kinetic Inductance Detectors*, Ph.D. thesis, California Institute of Technology (2004).
12. J. Gao, M. Daal, A. Vayonakis, S. Kumar, J. Zmuidzinas, B. Sadoulet, B. A. Mazin, P. K. Day, and H. G. Leduc, *Appl. Phys. Lett.* **92**, 152505 (2008).
13. B. Mazin, S. McHugh, A. Merrill, J. Martinis, D. Sank, and E. Lucero, *APL* (in preparation).
14. M. Daal, B. Sadoulet, and J. Gao, *J Low Temp Phys* **151**, 544–549 (2008).
15. S. Doyle, P. Mauskopf, J. Zhang, S. Withington, D. Goldie, and D. Glowacka, *This Proceeding* (2009).

16. O. Noroozian, P. Day, J. Gao, J. Glenn, S. Golwala, H. LeDuc, P. Maloney, B. Mazin, J. Sayers, J. Schlaerth, A. Vayonakis, and J. Zmuidzinas, *This Proceeding* (2009).
17. J. Gao, J. Zmuidzinas, B. A. Mazin, H. G. Leduc, and P. K. Day, *Appl. Phys. Lett.* **90**, 102507 (2007).
18. J. Gao, M. Daal, J. M. Martinis, A. Vayonakis, J. Zmuidzinas, B. Sadoulet, B. A. Mazin, P. K. Day, and H. G. Leduc, *Appl. Phys. Lett.* **92**, 212504 (2008).
19. S. Kumar, J. Gao, J. Zmuidzinas, B. A. Mazin, H. G. Leduc, and P. K. Day, *Appl. Phys. Lett.* **92**, 123503 (2008).
20. K. E. Gray, *J. Phys. F: Metal Phys.* **1**, 290–308 (1971).
21. S. Yates, and J. Baselmans, *This Proceeding* (2009).
22. R. Barends, S. van Vliet, J. J. A. Baselmans, S. J. C. Yates, J. R. Gao, and T. M. Klapwijk, *Phys Rev B* **79**, 020509 (2009).
23. S. Yates, A. Baryshev, J. Baselmans, B. Klein, and R. Gusten, *Appl Phys Lett* **Accepted** (2009).
24. J. Schlaerth, A. Vayonakis, P. Day, J. Glenn, J. Gao, S. Golwala, S. Kumar, H. Leduc, B. Mazin, J. Vaillancourt, and J. Zmuidzinas, *J Low Temp Phys* **151**, 684–689 (2008).
25. P. Maloney, N. Czakon, P. Day, J. Gao, J. Glenn, L. H. Golwala, S., B. Mazin, D. Moore, O. Noroozian, H. Nguyen, J. Sayers, J. Schlaerth, J. Vaillancourt, A. Vayonakis, and J. Zmuidzinas, *This Proceeding* (2009).
26. N. Czakon, A. Vayonakis, J. Schlaerth, M. Hollister, S. Golwala, P. Day, J. Gao, J. Glenn, H. LeDuc, P. Maloney, O. Noroozian, H. Nguyen, J. Sayers, J. Vaillancourt, and J. Zmuidzinas, *This Proceeding* (2009).
27. S. Yates, J. Baselmans, A. Baryshev, A. Neto, G. Gerini, R. Barends, and Y. Lankwarden, *This Proceeding* (2009).
28. G. J. Grabovskij, L. J. Swenson, O. Buisson, C. Hoffmann, A. Monfardini, and J. C. Villegier, *Appl. Phys. Lett.* **93**, 134102 (2008).
29. D. Moore, B. Mazin, S. Golwala, B. Bumble, J. Gao, B. Young, S. McHugh, P. Day, H. LeDuc, and J. Zmuidzinas, *This Proceeding* (2009).
30. S. Golwala, J. Gao, D. Moore, B. Mazin, M. Eckart, B. Bumble, P. Day, H. G. LeDuc, and J. Zmuidzinas, *J Low Temp Phys* **151**, 550–556 (2008).
31. J. Schlaerth, S. Golwala, J. Zmuidzinas, A. Vayonakis, J. Gao, N. Czakon, P. Day, J. Glenn, M. Hollister, H. LeDuc, P. Maloney, B. Mazin, H. Nguyen, J. Sayers, and J. Vaillancourt, *This Proceeding* (2009).